Experimental setup

In this work we have chosen the standard approach for providing the biochemical support to the structural implications in which the predictions generated based on the *T. thermophilus* RNAP/dMyx complex structure were verified by the biochemical *in vitro* experiments carried out on the homologous *E. coli* system. Such an approach is commonly accepted, was successfully utilized in the overwhelming majority of the reported studies of the bacterial transcription[1-4], and (to our knowledge) never caused any notable artifacts. Moreover, in the present studies it has a number of the apparent advantages over the alternative approach of carrying out both structural and biochemical experiments on the same system, i. e. *T. thermophilus*.

First, obtaining the biochemical results in *E. coli* using the predictions based on the *T. thermophilus* RNAP structure substantially strengthens the mechanistic implications of the work and puts them in a more general stream.

Second, our studies led to identification of an apparent intermediate in open complex formation; this conclusion can only be drawn if one uses a model system in which this mechanism has been characterized in some detail (definitely not *Thermus*). For this reason, we used the lambda P_R promoter that has been studied by many labs for years[5-9], and the intermediates in open complex formation have been characterized kinetically and probed by footprinting[10] – thus we have the reference dataset in which the pattern is known to a single nucleotide resolution.

Finally, if one has an ultimate goal of designing new clinical drugs, *Thermus* is indeed a

wrong model system; conversely, *E. coli* and its close relatives are among the most prominent pathogens; in any case, a promising antibiotic should be a broad spectrum one.

Towards improvement of the antibiotic activity

Our structural analysis suggests that the affinity of dMyx to RNAP might rely on the competition of dMyx with the original (presumably more stable) configuration of the switch-2 segment. Thus, one way to improve the inhibitory properties of the antibiotic is to modify the compound to enhance its binding to RNAP in the major binding site. For example, the structure shows that the highly conserved residue Eβ1041 (*T. thermophilus* sequence) forms the hydrogen bonds with N1 and O5 (Fig. 1d) of dMyx. Since the Glu side chain is likely negatively charged at a physiological pH, substitution of O5 for N in dMyx might increase the binding affinity of antibiotic to RNAP. Another way is to design a derivative with the additional group(s) that would clash with the switch-2 residues in the original configuration thereby making the antibiotic more competitive. Substitution of the dMyx O3 oxygen (Fig. 1d) with some bulky aliphatic group may make the inhibitor substantially more competitive: this group would occupy the open space at the entry of the dMyx binding site while the switch-2 segment adopts the refolded (open) conformation (Supplementary Fig. 8b) and would severely clash with the original (closed) configuration of switch-2 (Supplementary Fig. 8a).

dMyx likely stabilizes rather than induces the switch-2 refolding

The switch-2 conformation observed in the RNAP/dMyx complex might be induced by dMyx and fixed only in presence of the antibiotic. In this scenario, this conformation could play no essential physiological role during formation of transcription initiation complexes in the absence of dMyx. However, several considerations argue that, in contrast, the switch-2 refolding is a prerequisite for the dMyx binding, suggesting in turn that the refolded switch-2 configuration may occur in the antibiotic-free RNAP and is therefore physiologically relevant.

First, dMyx binding likely requires switch-2 refolding because even a partial insertion of dMyx into its binding site, which in principle could initiate the switch-2 conformational transition, is blocked in its original configuration (Supplementary Fig. 8a). Consistently, substitutions that favor refolding confer hypersensitivity (see main text). Thus, to induce the alternate switch-2 conformation, dMyx presumably should first bind somewhere near (but not overlapping with) its major binding site and interact with switch-2 to promote its refolding. Given that dMyx is hydrophobic, this putative "pre-insertion" site should be largely hydrophobic and complement in shape to some unique portion of the antibiotic to distinguish it from other compounds. However, our modeling does not reveal any site that could play such a role. In particular, the RNAP surface near the switch-2 segment at the entrance into the major dMyx binding site appears substantially charged (Supplementary Fig. 12).

Second, changes in the switch-2 designed to promote its re-folding stabilize promoter complexes in states different from the properly formed, active open complexes (Fig. 4); these complexes, however, become transcriptionally active upon addition of substrates. In

particular, β'Δ338-341 RNAP that, unlike dMyx-bound wild-type RNAP, retains substantial transcriptional activity (a property necessary for assaying its sensitivity to dMyx) is both dMyx-hypersensitive (Fig. 2) and is stabilized apparently in the same (by footprinting criteria) state as the dMyx-bound enzyme (Fig. 4 and Supplementary Fig. 11). In other words, although the deletion mimics the effects of dMyx by stabilizing the unproductive configuration of the promoter complex, this effect is reversed in presence of the NTP substrates which would shift the equilibrium towards the catalytically competent state. Similar on-pathway intermediates that give rise to active complexes have been trapped by altering reaction conditions[5,11,12] or a large deletion in β-subunit[13].

Supplementary Table 1. Data collection and refinement statistics.

Data collection	
Space group	$P6_5$
Unit cell parameters (Å)	$a = b = 235.0$, $c = 255.0$
Resolution (Å)	40.0-2.7 (2.80 – 2.70)*
Reflections (Total/Unique)	1102413/212777
I/σ(I)	14.3 (2.5)
R_{merge} (%)	8.4 (44.4)
Completeness (%)	97.7 (93.2)
Refinement	
Space group¶	$P3_2$
Twinning (%)	50.0
Twinning operator	-h,-k,l
Resolution (Å)	40.0–2.7 (2.80 – 2.70)
Reflections used	422394
R_{factor} (%)	24.0 (29.9)
R_{free} (%)	27.0 (32.3)
Overall B-factor/RMSD (Å^2)	57.6/1.6
Cross-validated sigma-A coordinate error (Å)	0.44
Number of protein atoms	52790
Number of water molecules	4496
Number of dMyx atoms	60
Number of Zn^{2+} ions	4
Number of Mg^{2+} ions	2
Model quality	
RMSD bond length (Å)	0.015
RMSD bond angles (°)	1.99
RMSD improper angles (°)	1.22
Ramachadran plot	
	Number of residues (%)
Most favorable regions	84.6
Allowed region	15.1
Generously allowed regions	0.3
Disallowed region	0.0

$R_{merge}=\Sigma_{hkl}\Sigma_j | I_j(hkl) - \langle I(hkl)\rangle | / \Sigma_{hkl}\Sigma_j \langle I(hkl)\rangle$, where $I_j(hkl)$ and $\langle I(hkl)\rangle$ are the intensity of measurement *j* and the mean intensity for the reflection with indices *hkl*, respectively. $R_{factor,\ free}=\Sigma_{hkl}|\,|F_{calc}(hkl)| - |F_{obs}(hkl)|\,| / \Sigma_{hkl}|F_{obs}|$, where the crystallographic R-factor is

calculated including and excluding reflections in the refinement. The free reflections constituted 5% of the total number of reflections. RMSD – root mean square deviation. $I/\sigma(I)$ – ratio of mean intensity to a mean standard deviation of intensity. *The data for the highest resolution shell are shown in brackets.

¶The refinement was first carried out in the $P6_5$ space group. However, although the procedure of zonal scaling provided a substantially better match between the experimental and model structure factor amplitude, we were still unable to obtain an R-factor below 35.6% at 2.7Å resolution, whereas the EC map remained quite noisy albeit showing the clear ED in the protein and "omit" regions. Inability to improve the R-factor and to provide a high quality ED suggested that the data are likely affected by merohedral twinning, as was also observed in other projects in our lab[1,14-18]. Indeed, the calculations of the intensity statistics proposed by Yeates[19] and implemented in the CNS program[20] indicated a presence of the perfect merohedral twinning, thereby suggesting that a proper space group of the crystals is $P3_2$, rather than $P6_5$. At the same time, the fact that we still have been able to obtain an interpretable ED using the phases calculated in the $P6_5$ space group led us to conclude that, as observed previously[1,14-18], merohedral twinning mimicking the $P6_5$ space group is likely coupled with the non-crystallographic symmetry that also closely resembles the $P6_5$ crystallographic symmetry operators.

Therefore, to obtain the high quality of the ED, we have carried out the twinning refinement in the $P6_5$ space group using the CNS program[20]. For this, before the refinement we have expanded the crystallographic data processed in the $P6_5$ space group to that of $P3_2$ and have generated the two molecules initially related by the corresponding crystallographic symmetry operator. The rigid body twinning refinement using the two molecules in the $P3_2$ space group converged from the initial value of 35.6% to ~30.7% at 2.7Å resolution. The resulting $|2F_{obs} - F_{calc}|$ ED map was of substantially better quality than the one obtained for the $P6_5$ space group and allowed us to improve the model and to easily refine the structure to the crystallographic standards corresponding to the 2.7Å resolution data.

Supplementary References

1. Artsimovitch, I. et al. Allosteric modulation of the RNA polymerase catalytic reaction is an essential component of transcription control by rifamycins. *Cell* **122**, 351-63 (2005).
2. Campbell, E.A. et al. Structural, functional, and genetic analysis of sorangicin inhibition of bacterial RNA polymerase. *Embo J* **24**, 674-82 (2005).
3. Tuske, S. et al. Inhibition of bacterial RNA polymerase by streptolydigin: stabilization of a straight-bridge-helix active-center conformation. *Cell* **122**, 541-52 (2005).
4. Vassylyev, D.G. et al. Structural basis for transcription inhibition by tagetitoxin. *Nat Struct Mol Biol* (2005).
5. Craig, M.L. et al. DNA footprints of the two kinetically significant intermediates in formation of an RNA polymerase-promoter open complex: evidence that interactions with start site and downstream DNA induce sequential conformational changes in polymerase and DNA. *J Mol Biol* **283**, 741-56 (1998).
6. Hawley, D.K. & McClure, W.R. In vitro comparison of initiation properties of bacteriophage lambda wild-type PR and x3 mutant promoters. *Proc Natl Acad Sci U S A* **77**, 6381-5 (1980).
7. Kainz, M. & Roberts, J.W. Kinetics of RNA polymerase initiation and pausing at the lambda late gene promoter in vivo. *J Mol Biol* **254**, 808-14 (1995).
8. Leirmo, S., Harrison, C., Cayley, D.S., Burgess, R.R. & Record, M.T., Jr. Replacement of potassium chloride by potassium glutamate dramatically enhances protein-DNA interactions in vitro. *Biochemistry* **26**, 2095-101 (1987).
9. Roe, J.H. & Record, M.T., Jr. Regulation of the kinetics of the interaction of Escherichia coli RNA polymerase with the lambda PR promoter by salt concentration. *Biochemistry* **24**, 4721-6 (1985).
10. Davis, C.A., Bingman, C.A., Landick, R., Record, M.T., Jr. & Saecker, R.M. Real-time footprinting of DNA in the first kinetically significant intermediate in open complex formation by Escherichia coli RNA polymerase. *Proc Natl Acad Sci U S A* **104**, 7833-8 (2007).
11. Suh, W.-C., Ross, W. & T., R.M. Two Open Complexes and a Requirement for Mg2+ to Open the lambdaPR Transcription Start Site. *Science* **259**, 358-361 (1993).

12. Chen, Y.F. & Helmann, J.D. DNA-melting at the Bacillus subtilis flagellin promoter nucleates near -10 and expands unidirectionally. *J Mol Biol* **267**, 47-59 (1997).

13. Severinov, K. & Darst, S.A. A mutant RNA polymerase that forms unusual open promoter complexes. *Proc Natl Acad Sci U S A* **94**, 13481-6 (1997).

14. Perederina, A. et al. Regulation through the secondary channel--structural framework for ppGpp-DksA synergism during transcription. *Cell* **118**, 297-309 (2004).

15. Symersky, J. et al. Regulation through the RNA polymerase secondary channel. Structural and functional variability of the coiled-coil transcription factors. *J Biol Chem* **281**, 1309-12 (2006).

16. Temiakov, D. et al. Structural basis of transcription inhibition by antibiotic streptolydigin. *Mol Cell* **19**, 655-66 (2005).

17. Vassylyev, D.G. et al. Crystal structure of a bacterial RNA polymerase holoenzyme at 2.6 A resolution. *Nature* **417**, 712-9 (2002).

18. Vassylyeva, M.N. et al. Purification, crystallization and initial crystallographic analysis of RNA polymerase holoenzyme from Thermus thermophilus. *Acta Crystallogr D Biol Crystallogr* **58**, 1497-500 (2002).

19. Yeates, T.D. Detecting and overcoming crystal twinning. *Methods Enzymol* **276**, 344-358 (1997).

20. Brunger, A.T. et al. Crystallography & NMR system: A new software suite for macromolecular structure determination. *Acta Crystallogr D Biol Crystallogr* **54**, 905-921 (1998).

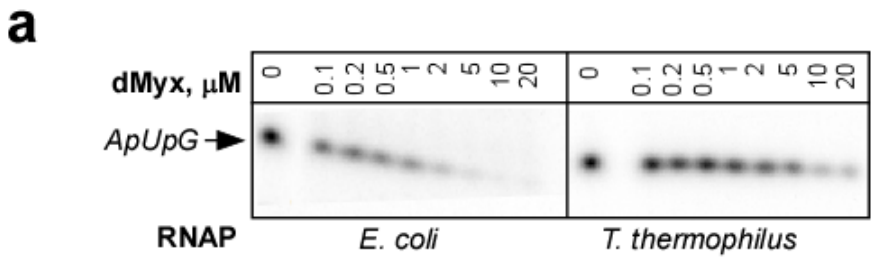
a
dMyx, μM
0
0.1
0.2
0.5
1
2
5
10
20
ApUpG
RNAP
E. coli
T. thermophilus

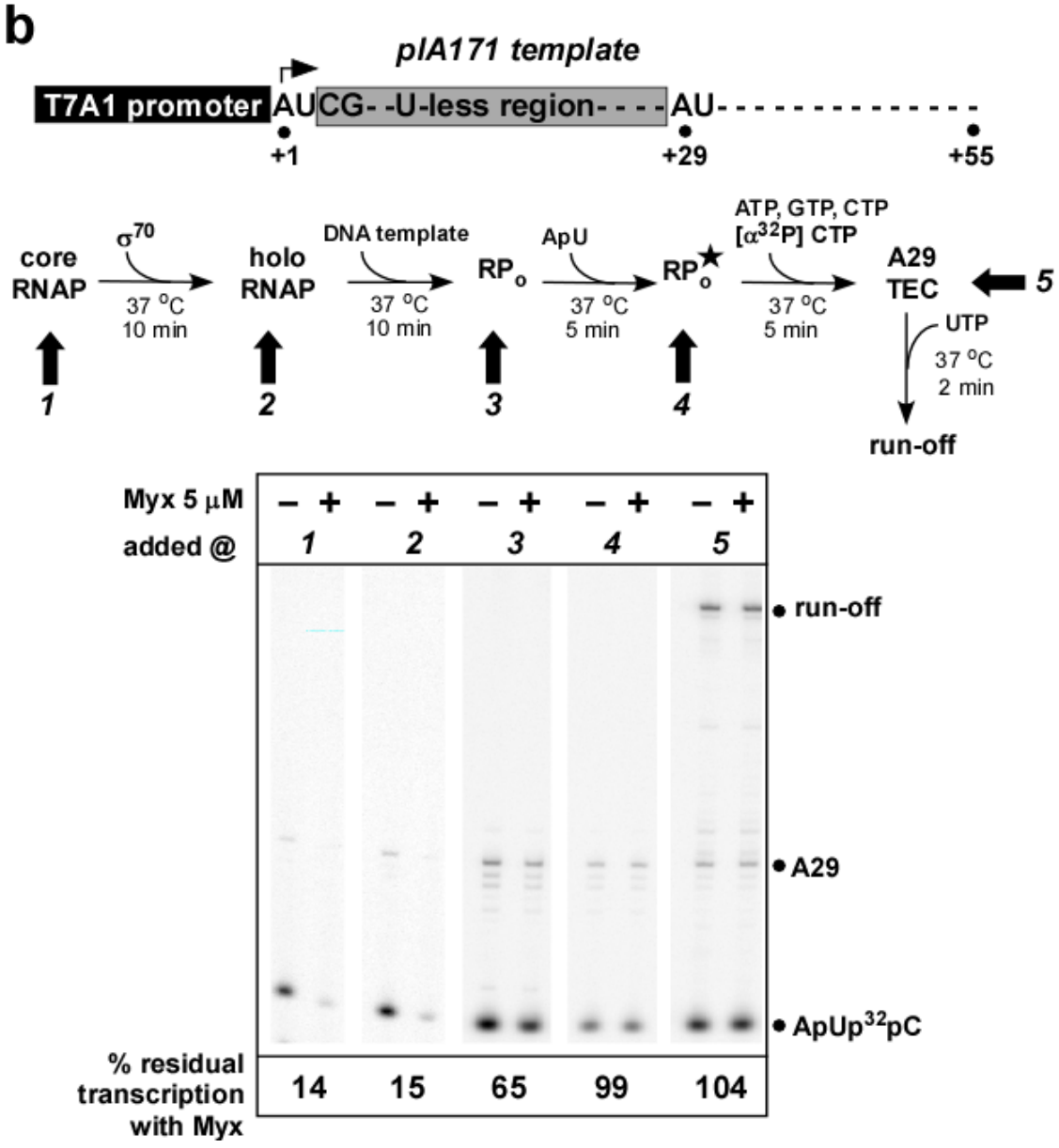
b
pIA171 template
T7A1 promoter
AUCG- -U-less region- - - -AU- - - - - - - - - - - - - -
+1
+29
+55
core RNAP
σ70
37 °C
10 min
holo RNAP
DNA template
37 °C
10 min
RPo
ApU
37 °C
5 min
RPo★
ATP, GTP, CTP
[α32P] CTP
37 °C
5 min
A29 TEC
5
UTP
37 °C
2 min
run-off
1
2
3
4
Myx 5 μM
– + – + – + – + – +
added @
1 2 3 4 5
run-off
A29
ApUp32pC
% residual transcription with Myx
14 15 65 99 104

Supplementary Figure 1. Myxopyronin inhibits transcription initiation by bacterial RNAPs. **a,** *E. coli* and *T. thermophilus* enzymes are inhibited by myxopyronin, as assayed by the Steady-state abortive synthesis of ApUpG RNA. The inhibitor (diluted into 50% EtOH) was preincubated with 20 nM RNAP holoenzyme (*E. coli* or *T. thermophilus*) at the concentrations indicated above the gel for 10 min at 37°C or 55°C, respectively. A mix containing linear λP_R promoter (which is recognized efficiently by either enzyme) template obtained by PCR amplification of pIA226 (2 nM), ApU (100 μM), and [α^{32}P]-GTP in 20 mM Tris-acetate, 20 mM Na-acetate, 2 mM Mg-acetate, 5% glycerol, 1 mM DTT, 0.1 mM EDTA, pH 7.9 was pre-equilibrated at the target and added to the RNAP/inhibitor mixture, followed by a 15-min incubation at 37°C (*E. coli*) or 55°C (*T. thermophilus*). The reaction was quenched by addition of an equal volume of saturated urea in 90 mM Tris-borate, pH 8.3, 50 mM EDTA. Products were analyzed on a 7 M urea, 12% (w/v) acrylamide:bisacrylamide (19:1) denaturing gel. **b**, As a template, linear pIA171 template with a T7A1 promoter followed by a 29-nt long "U-less cassette" was used. The key features of this template are shown on top; the run-off transcript is 55-nt long. *E. coli* RNAP core and σ^{70} were used in these experiments. The point of dMyx addition was varied as indicated in the reaction schematic. In the reactions **1-4**, only three substrate NTPs were present, whereas UTP was omitted to allow formation of the transcription elongation complex halted prior to addition of UMP at position 30 (A29). In reaction **5**, all four NTPs were present, allowing formation of the full-length, run-off RNA. The reactions were quenched and analyzed as in **a**. We conclude that dMyx acts before the open promoter complex formation and cannot inhibit transcription if added after the stable open complex (RP_o★) is formed (reactions **4** and **5**). The "intermediate" effect in reaction **3** (dMyx added to RP_o) is likely due to the relative (*e.g.*, compared to λP_R) instability of RP_o formed at the T7A1 promoter; these complexes are at equilibrium with dMyx-sensitive closed and intermediate complexes. Thus, to form a "stable" RP_o★ complex, we added ApU primer to the RP_o in reaction **4**.

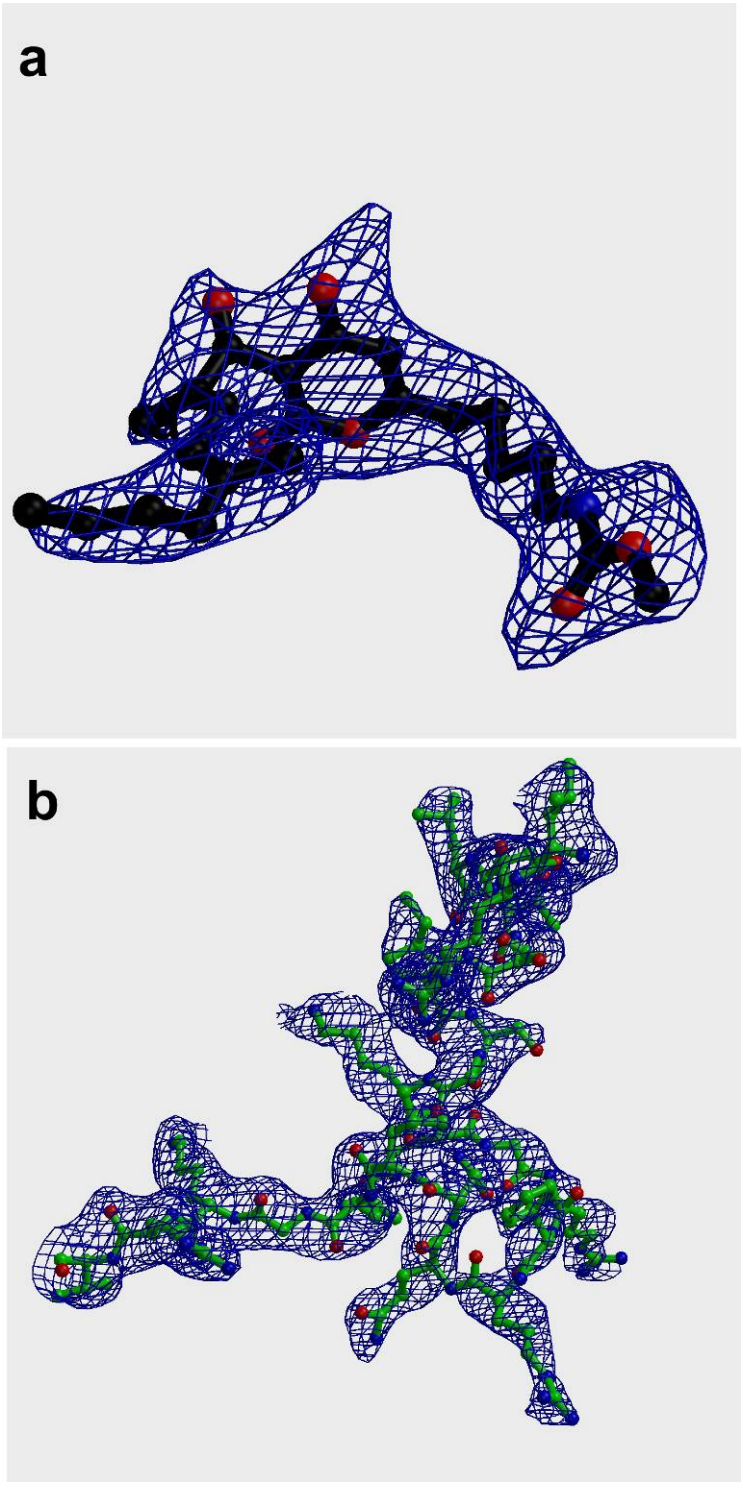

Supplementary Figure 2. The quality of the RNAP/dMyx structure. a, b, The final slow annealing (F_{obs}-F_{calc}) omit electron density (blue) for dMyx (3.0σ level) (**a**), and switch-2 segment (2.4σ level) (**b**) in the complex structure.

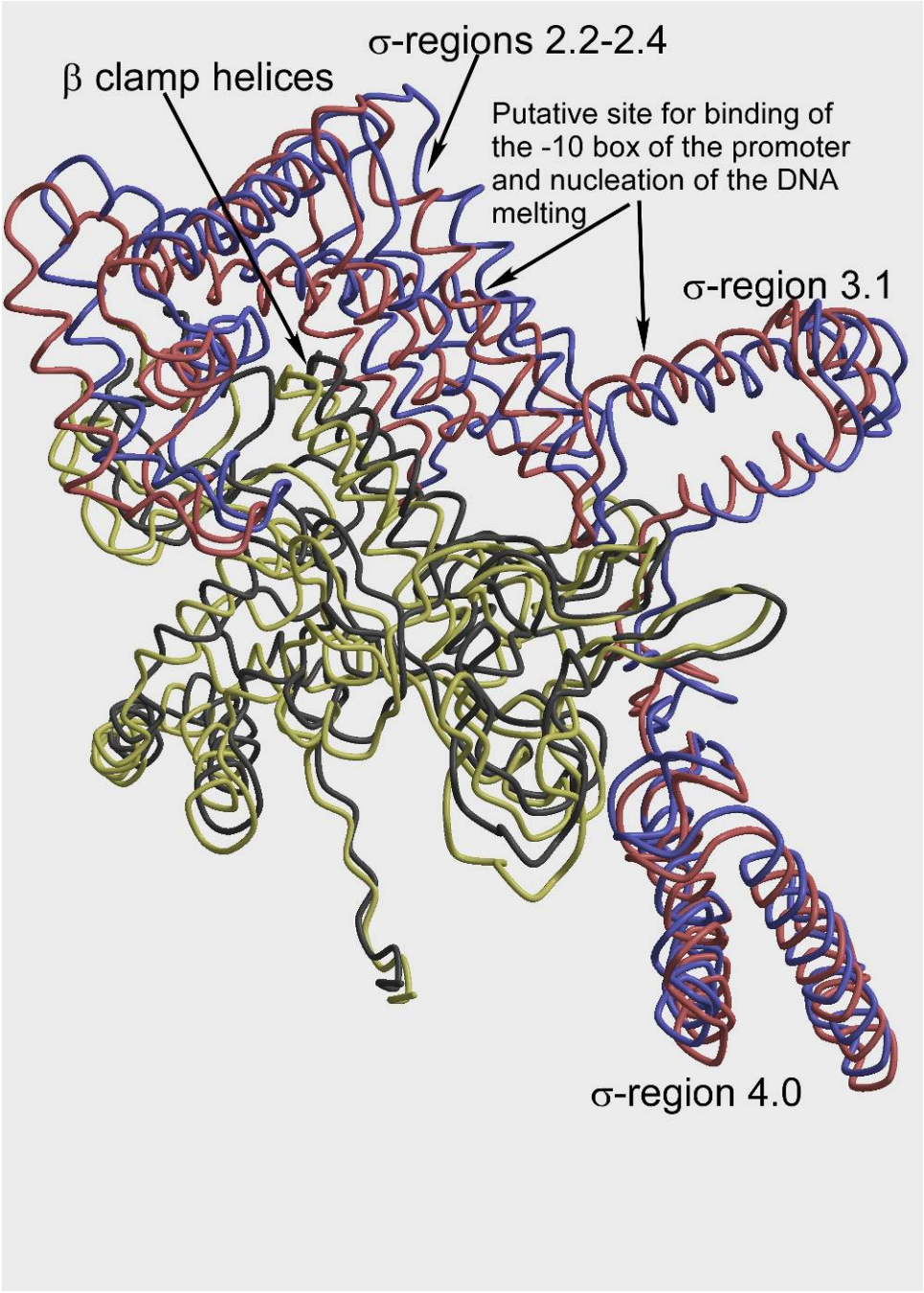

Supplementary Figure 3. The RNAP domain rearrangement induced by the dMyx binding. The N-terminal β'-subunit domains are shown in grey and yellow, while the σ-subunits are in blue and red for the RNAP/dMyx complex and dMyx-free RNAP, respectively.

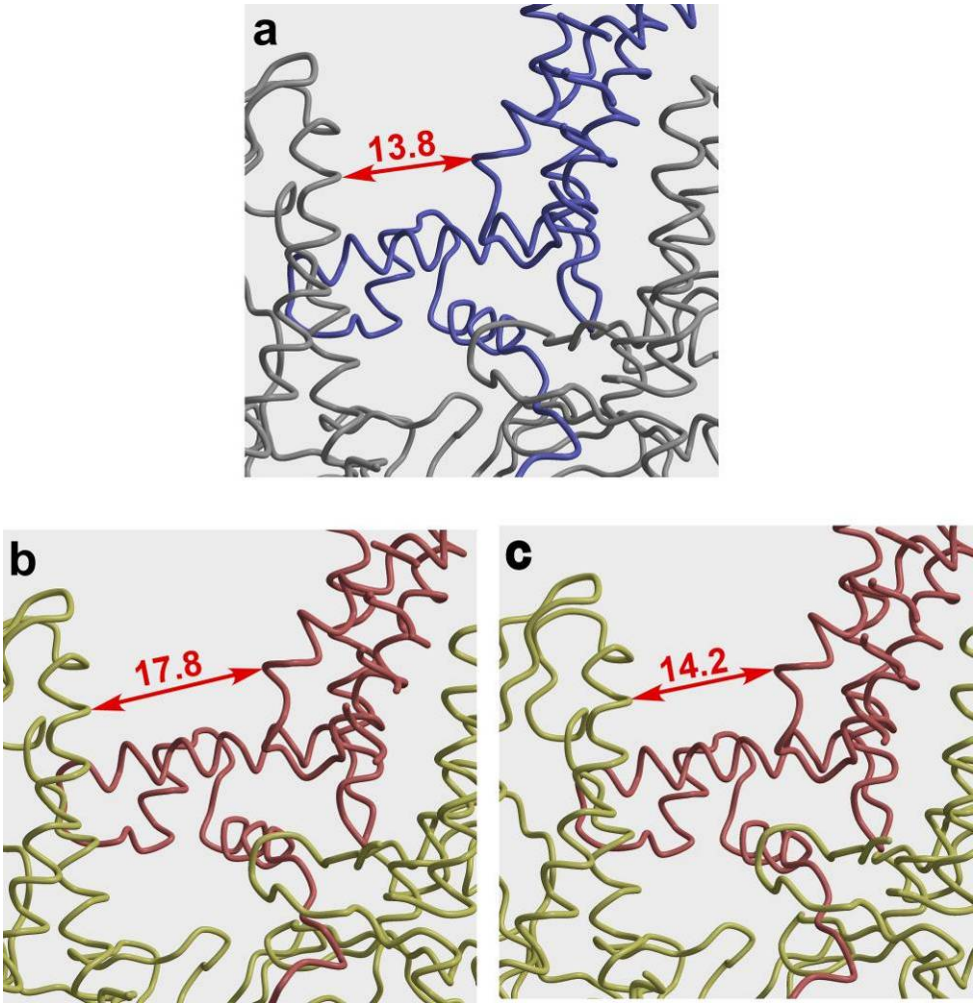

Supplementary Figure 4. The dimensions of the RNAP main channel in the RNAP/dMyx and apo-RNAP structures. The most narrow place of the channel is indicated by red arrows and distances in Å. **a,** RNAP/dMyx complex (σ-subunit – blue; core enzyme – grey). **b, c,** The apo-RNAP structure. The first (**b**) and second (**c**) crystallographically independent molecules are shown (σ-subunit –orange; core enzyme – yellow).

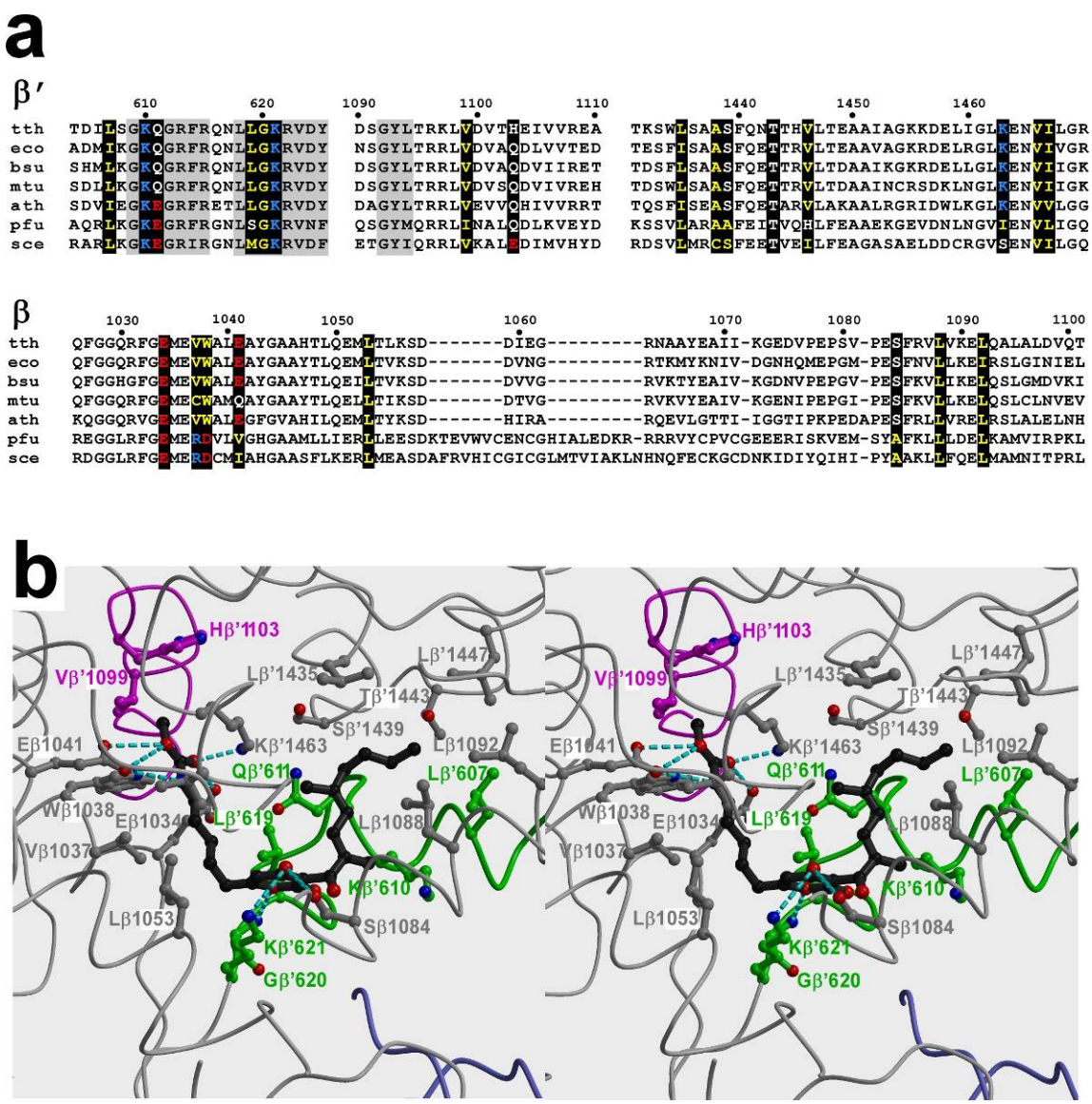

Supplementary Figure 5. The dMyx binding determinants in the RNAP/dMyx complex structure. a, Sequence alignment of the β and β'-subunit fragments containing the dMyx binding residues (marked by the black boxes) from bacterial (*E. coli*, Eco*; T. thermophilus*, Tt, *Bacillus subtilis*, Bsu; *Mycobacterium tuberculosis*, Mtu), archaeal (*Pyrococcus furiosis*, Pfu), chloroplasts (*Arabidopsis thaliana*, Ath) and yeast *Saccharomyces cerevisiae* (Sce) RNAPII enzymes. The residues are numbered (above the sequence) as in the *T. thermophilus* sequence. The hydrophobic, basic, acidic and polar residues are shown in yellow, blue, red and white, respectively. **b,** Stereo view of the dMyx (black) binding site. The hydrogen bonds between the protein residues and dMyx are shown by the cyan dashed lines.

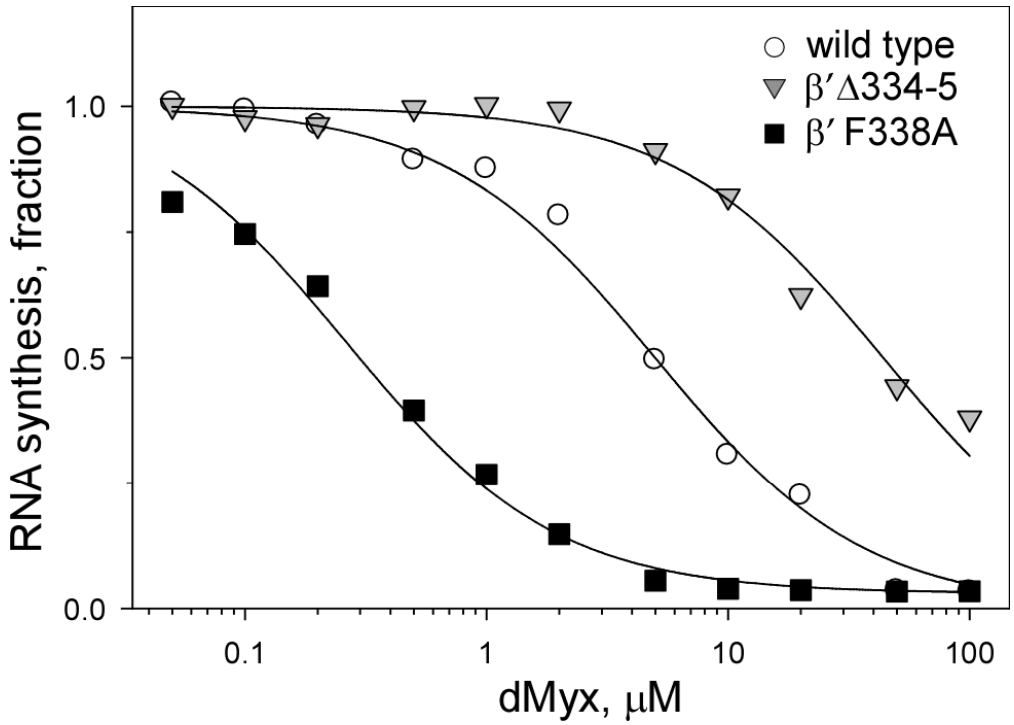

Supplementary Figure 6. Effects of dMyx on RNAP activity *in vitro*. The fraction of RNA synthesis (compared to 1 in the absence of dMyx) plotted against dMyx concentration for the wild-type, resistant (β' Δ334-335), and hypersensitive (β'F338A) recombinant *E. coli* enzymes (see Supplementary Methods for description).

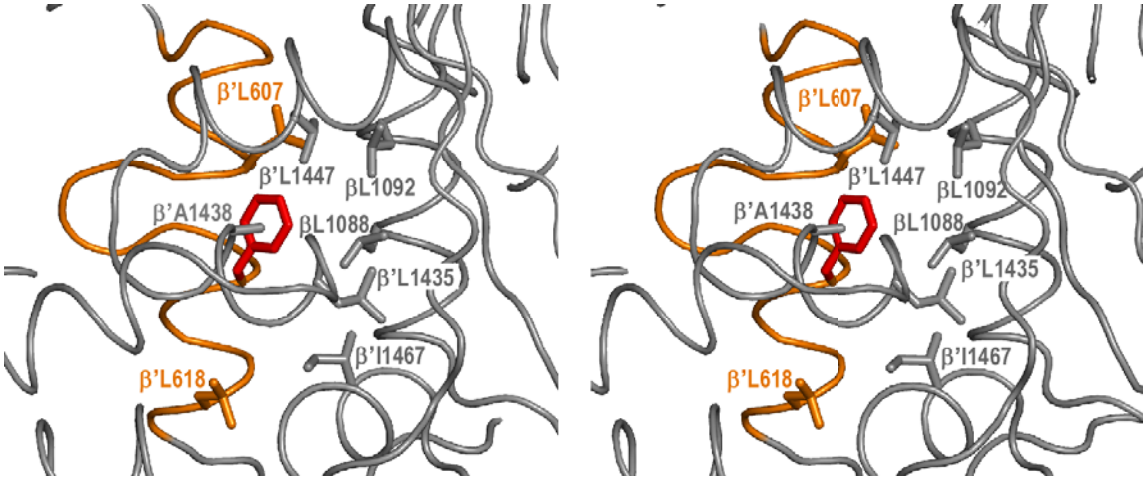

Supplementary Figure 7. Hydrophobic interactions stabilize the original switch-2 conformation. The side chain of Phe β'614 (red, β'338 in *E. coli*) from the switch-2 segment (orange) is inserted in the RNAP internal hydrophobic core (gray) thereby likely stabilizing the original conformation of the switch-2 segment and preventing isomerization of the flipped out residues (β'610-611) into an α-helical configuration observed in the RNAP/dMyx structure. The side chains are marked in orange or grey according to the corresponding RNAP region, β'F614 is shown in red and unmarked.

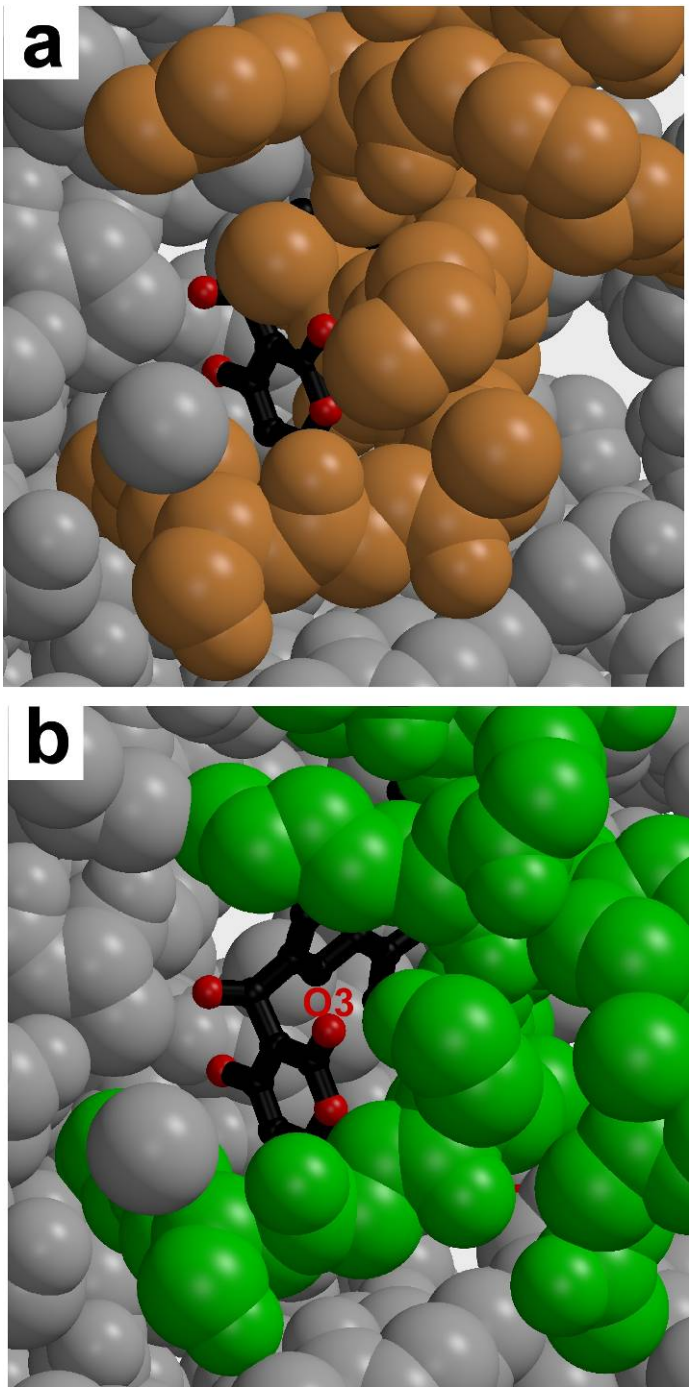

Supplementary Figure 8. The entry into the dMyx binding site. a, b, The closed (**a**) and open (**b**) configuration of the switch-2 motif in the apo-RNAP (orange) and RNAP/dMyx complex (green), respectively. In the closed state, dMyx access to its binding site appears largely blocked.

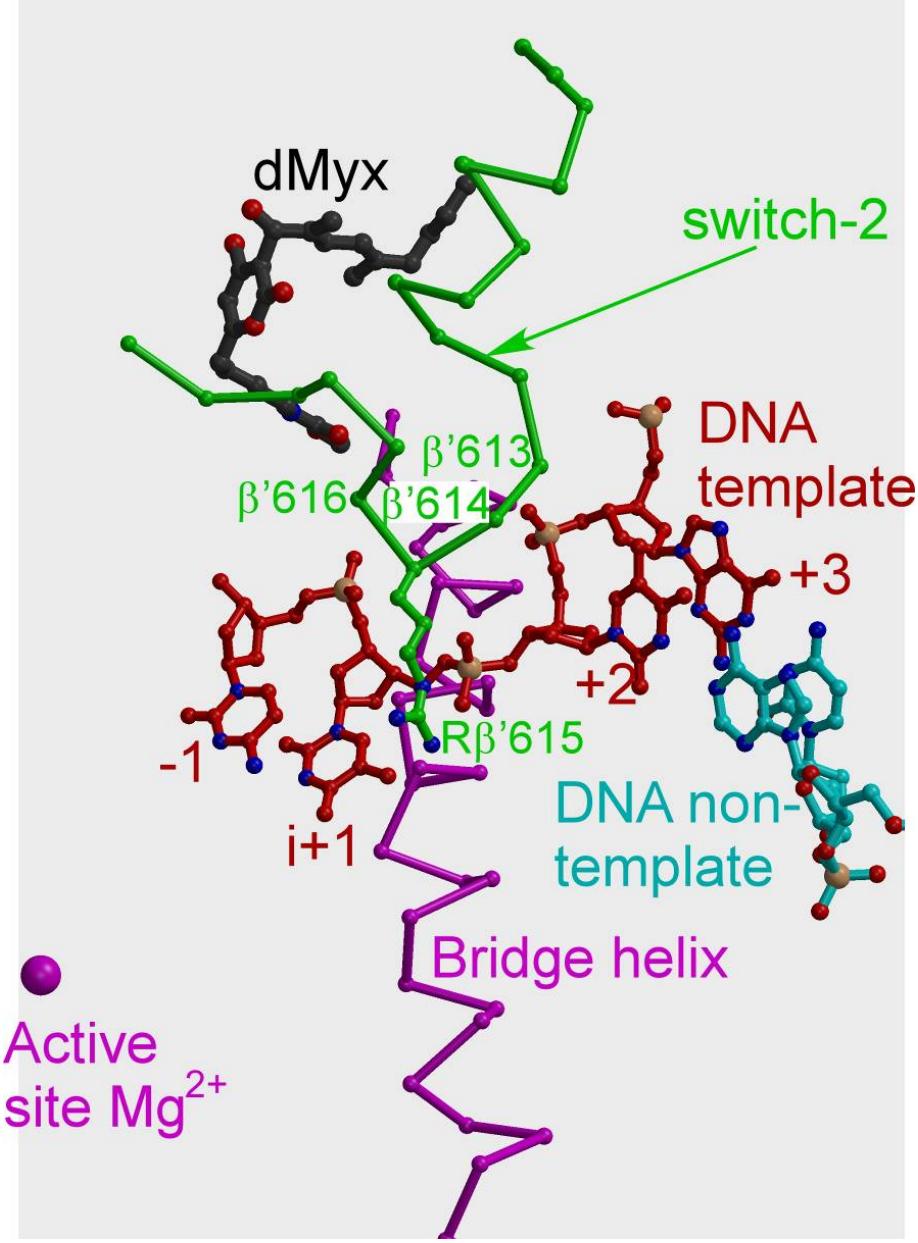

Supplementary Figure 9. Modeling of the DNA template to the RNAP/dMyx complex. The main chain of the residues located at the tip of the C-terminal loop of the refolded switch-2 segment (β'613-616) clash with phosphate backbone of the DNA template nucleotides in vicinity to the active site. In particular, the main and side chains of Arg β'615 appears to completely block access for the acceptor template base (i+1) to its binding site in the active transcription complex. Importantly, the resolution of the RNAP/dMyx structure is high enough for feasible modeling. Furthermore, the refolded switch-2 segment is well resolved, allowing us to predict the potential competition.

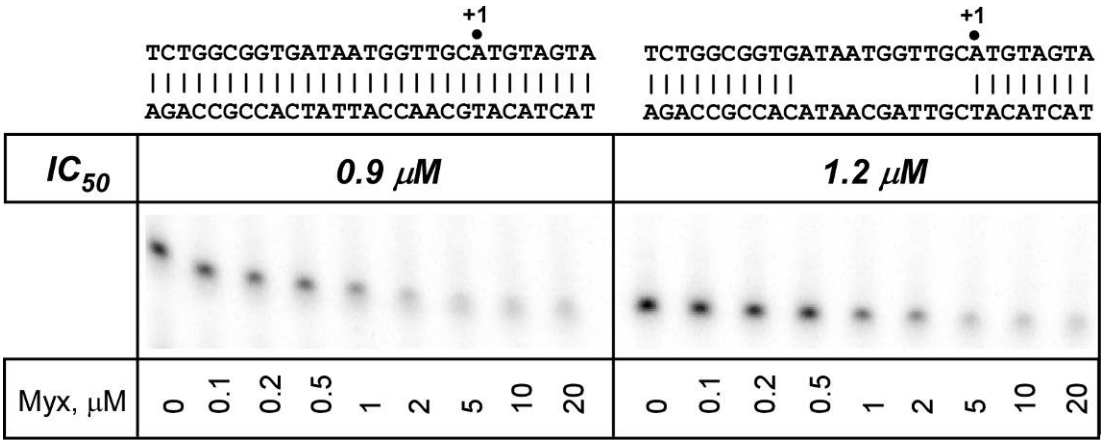

Supplementary Figure 10. Myxopyronin inhibits transcription from both the natural, double-stranded (left) or artificially melted (right) λP_R promoter templates. The melted region is indicated. Synthesis of ApUpG abortive RNA was followed as a function of the inhibitor concentration shown below each gel; the assays were carried out with the *E. coli* RNAP holoenzyme as described in the Supplementary Methods section.

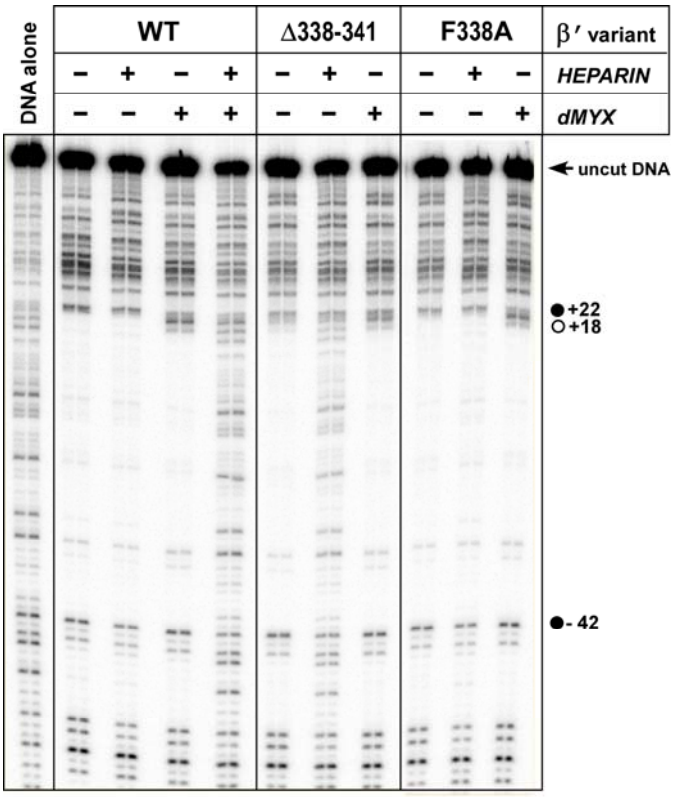

Supplementary Figure 11. DNaseI footprinting analysis of promoter complexes formed by switch-2 variants. A linear PCR fragment encompassing positions -81 through +70 of the λP_R promoter was generated with the [^{32}P]-labeled non-template DNA strand. The promoter fragment was incubated with the RNAP variant indicated above in the presence of 10μM dMyx or in the absence of the inhibitor (but with a mixture of EtOH/DMSO that is used as a dMyx solute); the leftmost lane contains no RNAP. After 15 min incubation at 37^{o}C, heparin was added to 10 μg/ml (where indicated) for 1 min, followed by DNaseI digestion (0.01U for 1 min). In the gel shown, independent reaction repeats were analyzed for consistency. The same upstream footprint boundaries (-42) were observed in all cases. In contrast, the downstream boundaries were altered by dMyx or a deletion in switch 2. Addition of dMyx shifted the downstream footprint boundary from +22 (black circle) to +18 (white circle). The Δ338-341 RNAP alone behaved similarly to the wild-type RNAP *in the presence* of dMyx: the deletion enzyme formed a heparin-sensitive promoter complex with the shortened downstream footprint even in the absence of the inhibitor. These data are consistent with the results of $KMnO_4$ probing (Fig. 4 in the main text), where the deletion enzyme displayed a pattern identical to the wild-type RNAP inhibited by the addition of dMyx.

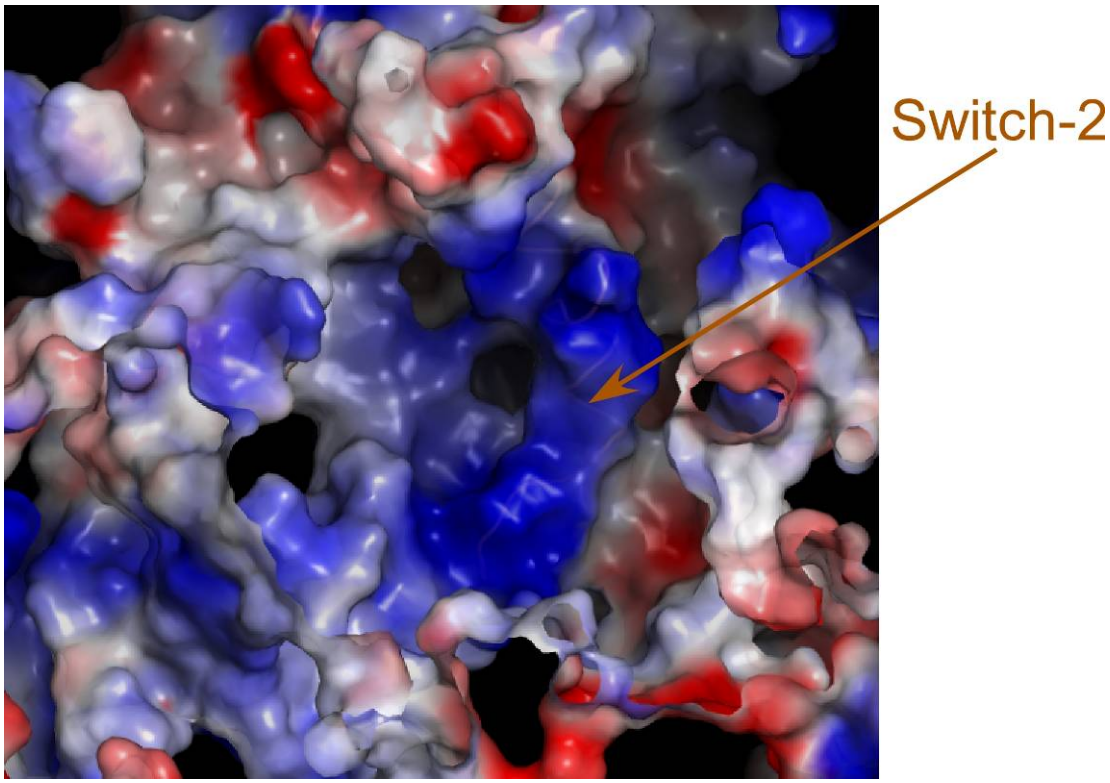

Supplementary Figure 12. The surface of the electrostatic potentials near the entry of the dMyx binding site. The negatively and positively charged and neutral regions are colored in blue, red, and white, respectively. The switch-2 segment is in the original (apo-RNAP) closed configuration. The view is similar to that of the Supplementary Fig. 8.